Cellular and Molecular Biology ™ **55**, N°3, 7-12
DOI 10.1170/T867

ISSN 1165-158X
2009 Cell. Mol. Biol.™

'VOXELIZATION' OF ALDERSON-RANDO PHANTOM FOR USE IN NUMERICAL DOSE MEASURING

A. M. SANTOS[1] ✉ AND J. W. VIEIRA[2, 3]

1Federal Center of Technological Education of Piauí, Liberdade Square, 1597, 64000-040, Teresina city, Piauí state, Brazil
✉ Fax : +55 086 3215-5209 email : adrimarcio.santos@gmail.com
2Federal Center of technological Education of Pernambuco, Av. Prof. Luiz freire, 500, Recife city, Pernambuco state, Brasil.
3Polytechnical School of Pernambuco, Benfica street, 455, Recife city, Pernambuco state, Brasil.

Received, September 1st 2008; Accepted October 1st, 2009; Published November 15th, 2009

Abstract – The use of computational models of the human body (anthropomorphic phantoms) assists in the estimation of the dose absorbed in organs or tissues of people exposed to sources of radiation which are external or internal to them. Nowadays, more realistic anthropomorphic phantoms are based on volume elements, well-known as voxels, and they are constructed from real images obtained through the scanning of people by Computed Tomography (CT) or Magnetic Resonance Imaging (MRI). The existence of artifacts in original images CT or MRI indicates the necessity of utilizing filtering processes before segmentation with the purpose of eliminating noises, improving contrasts and also to detect contours of organs regions. This study presents the methodology used for the creation of a phantom of voxels from tomographic images of Alderson-Rando (AR) physical phantom and the development of a computational model of exposure formed by phantoms resulting from "voxelization" of AR connected to Monte Carlo EGS4 code, added by algorithms to simulate radioactive sources in internal dose measuring.

Key words: Alderson-Rando, Phantoms, Voxels, Monte Carlo, Numerical Simulation

INTRODUCTION

Computational models of the human body (anthropomorphic phantoms) are essential tools in numerical dose measuring and are used to assist in the estimate of dose absorbed in organs or tissues of people exposed to the located sources of radiation at external or internal levels. Nowadays, more realistic anthropomorphic phantoms are based on volume elements are based on volume elements, the so-called voxels, and they are constructed from real images obtained through the scanning of people by Computed Tomography (CT) or Magnetic Resonance Imaging (MRI). The estimation of dose are carried through Monte Carlo (MC) simulation and for this purpose anthropomorphic phantom must be connected to a MC code, that it will be responsible for the simulation of transport of radiation through the phantom. This type of coupling model is denominated computational model of exposure or simply "model". This study presents the methodology adopted for the creation of Alderson-Rando phantom of virtual voxels (ARV), as well as, the development the computational model of exposure formed by ARV phantom and Monte Carlo EGS4 code.

MATERIALS AND METHODS

Alderson-Rando Physical Phantom

They are used for the detailed mapping of the distribution of doses and are composed of a natural human skeleton recovered with material radiological equivalent to the soft tissue, such densities were based on the measures of the standard man of ICRP 23 [3], updated by ICRP 89 [4]. The most common composition of this phantom contains fats, fluids, muscles and other tissues of the human body [7]. The Alderson-Radon's lungs are molded to simulate human lungs in an average state of breath.

The female adult (Figure 1), for example, is divided into 36 numbered slices 2.5 cm thick, each of them with small orifices distributed in a mesh, 3 or 1.5 cm away from one another, depending on the slice. The orifices have the function to accommodate the thermo-luminescent dosimeters (Figure 2) inside the phantom.

Acquisition of tomographic images

The set 3D was obtained by means of tomographic images of AR female phantom of the Laboratory of Metrology of Ionizing Radiations (LMRI), with scanning carried out in the Center of Nuclear Medicine of Pernambuco (CEMUPE), using a tomographic device of SeleCT/SP type, manufactured by the PICKER (Figure 3), and adjusted in a voltage of 120 KV, 178 mAs, field of 20 x 20 cm and a matrix of 512 x 512.

Improvement of tomographic images

The approaches to enhance the tomographic images are divided into two major categories: methods in the spatial domain and methods in the frequency domain. The term *spatial domain* refers to the plan of image itself and the approaches in this category are based on the direct

manipulation of pixels in an image. The techniques for the processing in the *frequency domain* are based on the modification of the *Fourier Transform* of an image.

Figure 1. Alderson-Rando female phantom of the Laboratory of Metrology of Ionizing Radiations (LMRI)

Figure 2. Slices and orifices of Alderson-Rando phantom used to accomodate thermo-luminescent dosemeters.

Figure 3. Tomographic device of CEMUPE used to obtain tomographic images of Alderson-Rando phantom.

For the construction of ARV phantom the methods of spatial domain were utilized, as follows: 1 – Elimination of noises of acquisition by means of medium image [2]; 2- Pre-segmentation, by utilizing filters of derivative for the detection of contours [2]; 3 – Manual segmentation of out going images. The methods of the process images mentioned in this study are implemented on the DIP (Digital Image Processing) software developed by the Group of Numeric Dosimetry.

Medium Image

Take a noisy image $g(x,y)$ formed by the additional of a noisy $\eta(x,y)$ on the original image $f(x,y)$, that is,

$$g(x,y) = f(x,y) + \eta(x,y) \tag{1}$$

Where the supposition is that in every pair of coordinates (x,y) the noisy is not correlated and has a medium value equal to zero. The variance of an x random variable with m medium its defined as $E\left[(x-m)^2\right]$, where $E[\ ]$ is the argument expected value. The covariance of the two random variables is defined as being x_i and x_j is defined as $E\left[(x_i - m_i)\cdot(x_j - m_j)\right]$. If the variables are not correlated, the covariance is zero.

The object of this procedure is to reduce the contents of noise, by adding a set of noisy images, $\{g_i(x,y)\}$. If the noise meets the above mention limitations, one can show that, if an $\tilde{g}(x,y)$ image is formed by taking the medium on K noisy images,

$$\tilde{g}(x,y) = \sum g_i(x,y)/K \tag{2}$$

Being that,

$$E\{\tilde{g}(x,y)\} = f(x,y) \tag{3}$$

And,

$$\sigma^2_{\tilde{g}(x,y)} = \sigma^2_{\eta(x,y)}/K \tag{4}$$

Where $E\{\tilde{g}(x,y)\}$ is the expected value of $\tilde{g}(x,y)$, and $\sigma^2_{\tilde{g}(x,y)}$ and $\sigma^2_{\eta(x,y)}$ are variances of $\tilde{g}(x,y)$ and of $\eta(x,y)$ respectively. The standard deviation in any points on the medium image points is,

$$\sigma_{\tilde{g}(x,y)} = \sigma_{\eta(x,y)}/\sqrt{K} \tag{5}$$

As K increases, the equations (4) and (5) indicate that the variability (noise) of values of the pixels in each location (x,y) decreases. As $E\{\tilde{g}(x,y)\} = f(x,y)$, it means that $\tilde{g}(x,y)$ gets closed to $f(x,y)$ when the number of noisy images utilized in the process of taking the medium increases.

Filters of Derivatives

The main objective of filters based on derivative (fine or sharp filters) is to enhance delicate details in an image or to improve details that had been blurred by error or natural effect of a particular method of image acquisition. The use of the sharp image varies and includes applications ranging from the printing and construction of electronic medical images for industrial inspection to the automatic orientation in military systems.

In the previous section, it was seen that the blurring of images can be carried out in the spatial domain taking the mean of pixels in a neighborhood. As the mean is analogous to the integration, it can be concluded that the sharpening is carried by the space differentiation.

Basically, the essence of the reply of a derived operator is proportional to the degree of discontinuity of image in the point where the

operator is applied. Thus, the differentiation of image improves extremities and other discontinuities (such as noises) and do not reach areas with slow variation in the values of the ash tones.

The derivatives of a digital function are defined in terms of differences. There are several ways to define these differences. However, it is demanded that any definition used for a first-order derivative:

(1) Must be zero in monotonous segments (areas of values of constant ash tones);

(2) Must be non-null at the beginning and in the end of a step or slope of ash tones;

(3) Must be non-null along the slopes

Similarly, any definition of second-order derivative:

(1) Must be zero in monotonous areas;

(2) Must be non-null at the beginning and at the end of step or slope of ash tones;

(3) Must be zero along the slopes of constant inclination.

Once it is being dealt with digital quantities, the values of which are finite, the maximum change of possible ash tones also is finite and the smallest distance along which changes may occur is between adjacent pixels. The basic definition of the first-class concept of a one-dimensional function $f(x)$ is the difference,

$$\partial f / \partial x = f(x+1) - f(x) \quad (6)$$

Similarly, one define a derivative of second order as the difference,

$$\partial^2 f / \partial x^2 = f(x+1) + f(x-1) - 2 \cdot f(x) \quad (7)$$

It can be verified that the two definitions meet the conditions established previously for the derivatives of first and second order.

EGS4 Code

System EGS (Electron-Gamma Shower) of computer codes is a package on general purpose for Monte Carlo simulation of the connected transport of electrons and photons in an arbitrary geometry. The system of codes EGS was formally introduced in 1978 as a package called EGS3. The history of these codes is described in the documentation of SLAC-210 [1].

Currently, there are two versions rather used of this system: the EGS4 [6] that simulates the transport of the radiation in an arbitrary geometry for particles with energies above few KeV and below some TeV, simulating physical processes such as: production of Bremsstrahlung, loss of energy applied to the loaded particles in discrete interactions, production of pairs, Compton scattering, coherent scattering (Rayleigh) and photoelectric effect; and the EGSnrc [5], that it is a platform with graphical interface for user and corrected some existing errors of programming in the EGS4. In this study EGS4 was used, with the following capacities and characteristics:

- The electron or photons transport can be simulated in any chemical element, substance or mixture, using available information at the PEGS4 file that, among other information, supplies the shock sections of these media in function of the incident energy from the particles;

- The user must supply the initial conditions to a given simulation. This constitutes the radioactive source. From this beginning, the particles are carried through a medium, utilizing MC techniques to make several decisions such as to calculate the free mean way between collisions of particles with atoms of the environment, choose a physical process among the ones provided for a given energy, to calculate, cumulatively, the energy deposited, etc.

General mathematical model of a radioactive source

In order for the results obtained in simulations to reproduce the real results, it is necessary to evaluate the characteristics of the event studied and to try to reproduce them. The first point to be verified is the geometry of the source. Thus, algorithms of a general source was developed to be placed in any position inside a phantom and to serve as base for the development of specific geometry as punctual, plane or volumetric sources. The mathematical model, hereby, described, has the following algorithms:

STEP 01: raffle three random numbers;

STEP 02: determine the position where the interaction will take place using the equation $x_i = XL_i \cdot (N_{min} + (N_{max} - N_{min}) \cdot Naleat_i)$, being x_i one of the x, y or z variables; XL_i the dimension of voxel in one of the x, y or z directions; N_{min} and N_{max} represent the maximum and minimum numbers of slices, lines and columns of a phantom and $Naleat_i$ the related random number with x, y and z directions, respectively;

STEP 03: identify voxel where the interaction occurred;

STEP 04: verify whether this voxel is of the source organ. If that is not the case, return to STEP 01;

STEP 05: calculate the directing cosines, responsible for the next interaction in the phantom.

Computational model of exposition

As already mentioned, to carry out the simulations, Code Carlo Monte + Voxels Phantom coupling is required, thus forming a computational model of exposition or simply model. The model developed in this study uses code EGS4 with Virtual Phantom Alderson-Rando connected.

The creation of this model goes through two distinctive phases:

PHASE 01: Construction of voxel phantoms, that is initiated with the acquisition of the tomographic images and the improvement of them and, finally, the re-sampling of 3D battery of the images developed;

PHASE 02: Adaptation of EGS4 file to recognize voxel phantoms created in Phase 01. The modified files to recognize ARV were AR.mor, AR.voxdef.mor, AR.code.mor, ARLIST.dat, and PEGS4.dat; for they have such information as identification of the organ; maximum numbers of slices, lines and columns; densities and limits of the organs and shock sections from the compounds of the phantom.

RESULTS AND DISCUSSION

Alderson-Rando Virtual Phantom

The processing of tomographic images of AR phantom to the construction of ARV phantom first utilized the spatial method of the medium image for the reduction of noises (Figure 4b), once that the images obtained had artifacts (Figure 4a).

The next step, after completing the process of reduction of noises, was to improve the contour of image. This procedure helps the process of manual segmentation, for, after its application, the limits of

regions with different densities become well-defined in the image.

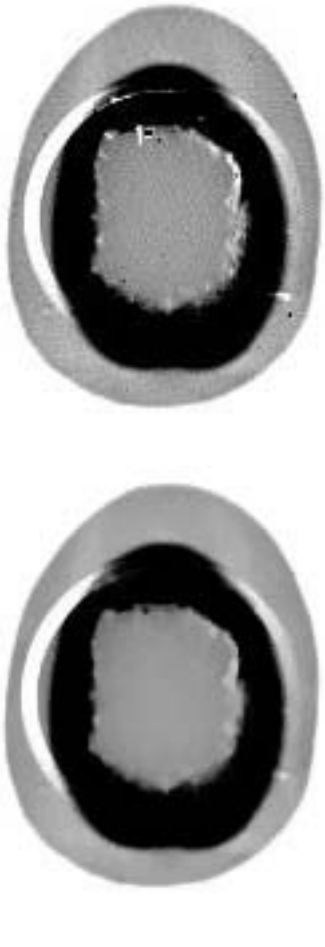

Figure 4. (**a**) - Original noisy image; (**b**) - Image treated by medium image method.

Figure 5 shows the prominence of contours of regions on the image of Figure 4b, obtained by means of the utilization of a filter of derivated called Sobel gradient. This kind of filter is indicated for situations where the definition of limits of regions with different tonalities, equivalent to this study.

Figure 5. Image treated with derivative filter of Sobel gradient.

In manual segmentation regions of volumes of each organ of phantom AR (lung, tissue soft and skeleton) were highlighted along with the selection of identification numbers for these regions. The resulting voxel phantom of the processes of segmentation and re-sampling is the ARV (Figure 6) with 320 slices, 436 columns, 258 lines and voxels in the format of a paving stone with 1.0 mm x 1.0 mm of base and 3 mm of height (slice).

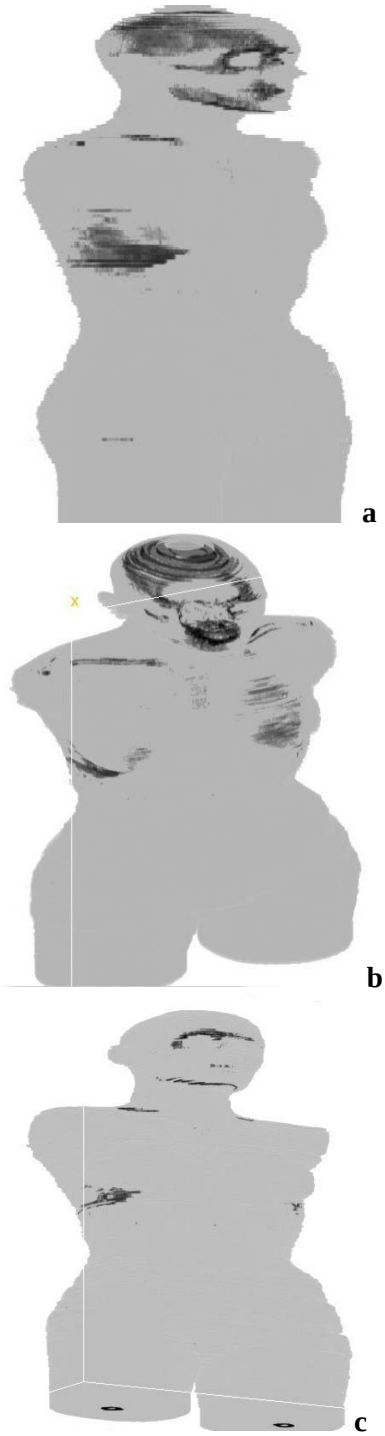

Figure 6. Sights of ARV Phantom, obtained with ImajeJ software.

Simulation with EGS4+ARV computational model of exposition

With model EGS4+ARV completed, some initial tests were carried out to verify the behavior of algorithm of the source which were developed and added to EGS4, and, observe whether the files of simulations outlets do not feature inconsistent results.

Test of the Number of Histories

This test consists of varying the number of histories of particles emitted by a source organ and verifying the behavior of the coefficients of variance (CV) of each organ. These coefficients vary for a $1/\sqrt{N}$ factor, being N the number of histories. Thus, one expects that increasing N implies in a reducing the values of CV.

In Table I the values of CV for three simulations carried out with different numbers of histories are listed.

Table I. Behavior of CV versus number of histories, for 600 keV energy.

Organs	CV (%)		
	N = 1 x 10^5	N = 5 x 10^5	N = 1 x 10^6
Soft Tissue	2.11	0.95	0.67
Lungs	0.03	0.02	0.01
Bones	9.60	4.35	3.12

The results presented in Table I was obtained for simulation, considering as source organ lungs of ARV and emitted particles (electrons) with average energy of 600keV. Table II e III show results of this test for electrons with 1.000 and 5.000 keV energy.

Table I.I. Behavior of CV versus numbers of histories, for 1000 keV and 5000 keV energies.

	N = 1 x 10^5	N = 5 x 10^5	N = 1 x 10^6
	CV (%) , Energy = 1000 keV		
Soft Tissue	1.51	0.68	0,48
Lungs	0.05	0.02	0.01
Bones	6.06	2.73	1.96
	CV (%) , Energy = 5000 keV		
Soft Tissue	0.64	0.28	0.20
Lungs	0.10	0.05	0.03
Bones	1.97	0.86	0.61

In these Tables, one can be notice that CVs had decreased with the increase of "N", indicating that the model is sensitive to variations of the number of histories.

Test of Deposited Energy

In this test simulations of different average energies of particles emitted by the source organ were made. For more energetic particles, the dose in the organs increases. The simulations were made for 600 keV, 1,000 keV and 5,000 keV energy values and a number of histories of N=1 x10 6 electrons.

In Table III are listed the results of accumulated dose in lungs and bones of the ARV.

Table III. Dose Accumulated in lung and bones of ARV for different energies.

Energy (keV)	Dose (mGy/ Bq s)	
	Lungs	Bones
600	2.08×10^{-11}	3.96×10^{-14}
1000	3.42×10^{-11}	13.96×10^{-14}
5000	15.03×10^{-11}	314.54×10^{-14}

The values listed in Tables from I to III indicate that coupling of voxels phantom ARV to Monte Carlo code EGS4 showed consistent results in the simulations. This stimulates the accomplishment of new studies developed through comparisons of the results obtained by for this model with the ones of other literatures available, in addition to experimental measures carried out in laboratories, using geometry that can be reproduced by the ARV+EGS4 computational model of exposure.

The calibration protocol developed in this work have shown to be of easy execution and more reliable than usual procedures since it uses all biokinetic parameters necessary for dose optimization. It is also important to point out that both the scintillation camera and the uptake probe can be used for the determination of the activity of ^{131}I in the thyroid of the patients.

This procedure can be applied for the individualized optimization of ^{131}I dose to be administered to each patient. Furthermore, this protocol presents additional advantages of convenience and reduced cost, since the patient will have to show up at the hospital only two times: a first one to perform the uptake test and a second to receive the therapeutic dose.

CONCLUSIONS AND PERSPECTIVES

In this study the algorithm of a general source was developed to be placed in any position inside the phantom and to serve as base for the development of specific geometry as punctual, plane or volumetric sources.

This source was added to Monte Carlo code EGS4 for simulation involving ARV phantom constructed from Alderson-Rando physical phantom, from the tomographic images to the EGS4+ARV coupling,

constituting thus, the computational model of EGS4+ARV exposure.

The algorithm of the general source, the steps for the construction of phantom of voxels, from a physical phantom and the EGS4+ARV model, illustrate the innovative character of this study and are contributions for studies in Numerical Dosimetry that require the development of a specific computational model for internal expositions and can be adapted for external exposures.

As perspectives for this study, the validation of ARV through experimental measures and comparisons with other models, in addition, can be cited the development of tools to automate (or semi-automate) the simulation process utilizing computational models of exposures that can be modified by the user, through an interface of data entries, manipulating such parameters as numbers of histories, source organs, among others.

ACKNOWLEDGEMENT

The Authors would like to express their gratitude to CEMUPE and LMRI. Thereby the construction of ARV was possible in the first place. The Authors also would like to acknowledge the 'Conselho Nacional de Desenvolvimento Científico e Tecnológico – CNPq' for the financial support.

REFERENCES

1. Ford, R. L., Nelson, W. R. The EGS code sistem: computer programmes for Monte Carlo simulation of electromagnetic cascades showers. Report n. SLAC-210, version 3. Stanford Linear Accelerator Center, Stanford University, Stanford, California, 1978.

2. Gonzalez, R. C., Woods, R. E. Digital Image Processing. 2ed, Prentice Hall, Upper Saddle River, New Jersey, USA, 2002, pp. 105-165.

3. ICRP 23. Report of the task group on reference man. International Commission on Radiological Protection, Pergamon Press, Oxford, 1975.

4. ICRP 89. Basic anatomical and physiological data for use in radiological protection: reference values. International Commission on Radiological Protection, Pergamon Press, Oxford, 2003.

5. Kawrakow, I., Mainegra-Hing, E., Rogers, D. W. O. EGSnrc. Disponível: <www.irs.inms.nrc.ca/inms/irs /EGSnrc/EGSnrc.html>, Access in February of 2008.

6. Nelson, W. R., Hirayama, H., Rogers, D. W. O. The EGS4 code-system. Report n. SLAC-235. Stanford Linear Accelerator, Stanford, California, 1985.

7. WHITE, D. R. Tissue substitutes in experimental radiation physics. *Med. Phys*., 1978, **5**(6), 467-479.

8. Araujo F., Rebelo A. M. O., Pereira A. C., Moura M. B., Lucena E. A., Dantas A. L. A., Dantas B. M. and Corbo R., Optimization of ^{131}I doses for the treatment of hyperthyroidism**.** *Cell. Mol. Biol*. 2009, **55**: 1-6.

9. Cardoso J. C. S., Berti e. A. R. and Xavier M., Whole-body measurements at IPEN, Brazil. *Cell. Mol. Biol*. 2009, **55**: 13-15.

10. Vieira J. W. and Lima F. R. A., a software to digital image processing to be used in the voxel phantom development. *Cell. Mol. Biol*. 2009, **55**: 16-22.

11. Holanda C. M. C. X., Silva-Júnior m. F., Alves R. C., Barbosa V. S. A., Silva R. P., Rocha L. G. and Medeiros A. C., The effect of the rochagan™ on radiolabeling with ^{99m}Tc. *Cell. Mol. Biol*. 2009, **55**: 23-28.

12. Oliveira C. M., Dantas A. L. A. and Dantas B. M., A methodology to evaluate occupational internal exposure to fluorine-18. *Cell. Mol. Biol*. 2009, **55**: 29-33.